The impact of land use change on runoff and peak flood discharges for the Nyando River in Lake Victoria drainage basin, Kenya

P. M. Kundu[1] & L. O. Olang[2]
[1]*University of Venda, Department of Hydrology and Water Resources, South Africa*
[2]*Department of Water and Environmental Engineering, Kenyatta University, Kenya*

Abstract

The effects of land use changes on the characteristics of floods in the Nyando River basin were investigated. Historical changes in the state of land cover were derived by processing multi-temporal Landsat images. The detected changes, together with other spatial datasets were subsequently used to estimate the physically based catchment and hydrologic model parameters for runoff generation and transformation, and for channel flow routing. The results obtained indicated that the basin experienced significant increases in peak discharge values, especially in the upstream areas where higher rates of deforestation were detected. Over the study period, the peak discharges increased by 16% in all of the 14 sub-catchments in the basin. Simulated flood volumes in the basin also increased by 10% over the same period. Based on the results obtained, the study outlined the consequences of land use change for flood events in the basin.
Keywords: land use change, peak floods, catchment, GIS, hydrological model.

1 Introduction

Land use changes in developing countries usually affect forests and national reserves. This is due to anthropogenic activities that create settlements which then bring about agricultural expansion that encroach on forest land. Poor hydrological measuring infrastructure and lack of expertise are amongst the

WIT Transactions on Ecology and The Environment, Vol 153,© 2011 WIT Press
www.witpress.com, ISSN 1743-3541 (on-line)
doi:10.2495/WS110081

major hindering factors towards comprehensive analyses of catchment scenarios and their impact on the environment (Kundu *et al.* [1]; Mutua and Klik [2]; Onyando *et al.* [3]. The Nyando River basin is among the five major basins in the Lake Victoria Development Basin (LVDB) and epitomizes the land degradation problem. Previous studies involving the use of multitemporal Landsat images of the basin revealed significant land cover changes and their impacts over the last four decades Luke *et al.* [4].

Due to insufficient hydrological data for model calibration and validation, this study relied more on the existing local and global geographical datasets involving rigorous use of GIS to parameterize the selected models using the method of Fürst [5]. Since different sub-catchments of the basin exhibited diverse spatio-temporal land changes, three general land cover scenarios were developed for the study.

2 The study area

The Nyando River basin shown in Figure 1 is located in Western Kenya between latitudes 0° 25′ S and 0°10′ N and longitudes 34° 50′ and 35° 50′ E and covers an area of about 3550 km^2. The basin is drained by the Nyando River which has a total length of about 170 km, and empties into the transboundary Lake Victoria at an altitude of about 1100 m a.m.s.l. The climate of the basin is largely influenced by the Equatorial Convergence Zone (ITCZ), modified by local orographic effects. Land use practises largely vary from planted forests interspersed with large scale tea plantations in the headwater catchment areas to commercial sugarcane plantations interspersed with small farm holdings in the central and lower parts of this basin.

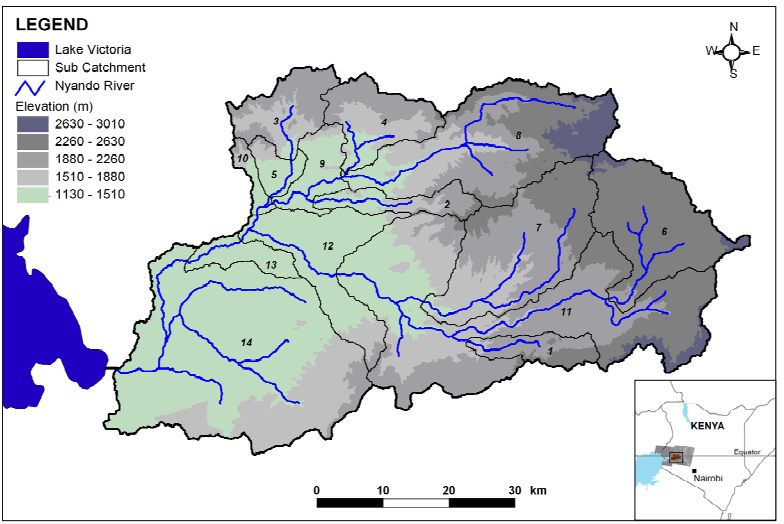

Figure 1: The study area and sub-catchments of the basin.

3 Materials and methods

3.1 Spatial data

Data on land cover and land use was obtained by detecting cover changes through classification and validation of selected multitemporal Landsat images between 1973 and 2008. It was done based on six predominant land cover classes including agriculture, forest, grassland, shrubland, wetland and water. The sub-catchments of the basin, their stream networks and the relevant topological and morphometric characteristics were derived from the global Shuttle Radar Topographic Mission (SRTM) digital elevation model (DEM). This was done within GIS based on the automated catchment delineation. Soils data was acquired from the Global Environment Facility Soil Organic Carbon database at http://www.isric.org and from the report by Batjes and Gicheru [6] on studies of carbon stocks and change in Kenya. Composite CN values for the sub-catchments were subsequently obtained from the CN grids of the basin through a zonal summary done in a GIS.

Previous studies in the basin documented the unreliability of stream flow data for use in a calibrated and validated hydrological modeling approach (Olang and Fürst [4]). This study, therefore, adopted an approach that treated the basin as ungauged, especially within the defined spatial units for the modeling. In order to study the possible bandwidth during floods, scenarios were assumed to apply equally to the sub-catchments. Similarly, the synthetic storm events selected for the study were also based on the rainfall magnitudes likely to cause floods in the basin. By comparing the results of scenarios within the respective sub-catchments with the land cover state in 2008, it was possible to evaluate the scenario that could reduce flood runoff within these regions.

To determine the effects of the land cover scenarios, four uniformly distributed synthetic storm events of depths 20 mm, 40 mm, 60 mm and 80 mm were applied to each sub-catchment. The storms were selected based on the general trends of the rainfall amounts predominant in the region, and assumed to have the same duration corresponding approximately to the time of concentration of each area. The longest flow path to the outlet and the average slopes of the catchments were obtained from a slope grid in GIS. The two parameters were used to determine the time of concentration.

3.2 Hydrological models

3.2.1 Generation and transformation of runoff

The Natural Resource Conservation Service – Curve Number model (NRCS-CN) [7] was used to estimate runoff volume. This was done based on standard CN tables for hydrological conditions, giving soil type and moisture conditions and the estimated direct runoff volume. The major assumption was that infiltration was less than or equal to the potential maximum retention as explained by Maidment [8]. Under these conditions, the model estimated the volume of runoff based on the ratios provided in eqn. (1).

$$\frac{F}{S} = \frac{Q}{P} \tag{1}$$

where, F is the infiltration, S is the maximum potential retention, Q is the actual runoff and P is the effective rainfall that potentially causes runoff.

The total precipitation is the sum of the runoff, the initial abstraction losses and infiltration losses. The runoff depth was then estimated from the relationship provided in eqn. (2).

$$Q = \left(\frac{(P - I_a)^2}{P - I_a + S} \right) \tag{2}$$

where, I_a is the initial abstraction.

Based on experiences from previous studies, the initial abstraction is typically assumed to be 20% of the maximum potential retention (S), which can be related to the mean curve number parameter, CN_m by eqn. (3).

$$S = \frac{25400}{CN_m} - 254 \tag{3}$$

Higher values of CN are usually construed to mean small rainfall losses and hence high runoff volume. The mean CN_m provided in Equation 3 represented values obtained under average antecedent soil moisture conditions (AMC, II). During flood conditions, it was quite often that the majority of the regions were under wet moisture condition (AMC, III). The conversion procedure provided by Chow *et al.* [9] was used to relate the two conditions based on adjustment factors.

Transformation of the generated runoff into corresponding runoff hydrograph at the outlet of the basin was achieved using the Clark's Unit Hydrograph (UH) model as described by the engineering manual (USACE, [10]). The translated hydrographs were then routed based on the linear reservoir concept to produce the instantaneous unit hydrograph (IUH) which represented the outflow from a single linear reservoir. The precipitation excess was assumed to occur with duration equal to zero such that the outflow was estimated using the impulse response function in eqn. (4).

$$O(t_0) = \frac{1}{K} e^{-\frac{t}{k}} \tag{4}$$

where, $O(t_0)$ is the rate of outflow from the reservoirs at time t_0; K is the storage coefficient and t is the time lag. A finite UH was then approximated by averaging the ordinates of the superimposed instantaneous unit hydrographs, lagged by a defined time step during the duration of the outflow using eqn. (5).

$$Q(t) = \sum_{i=1}^{n} \left(u\left[\Delta t,\ t - \Delta t(i-1) \right] I_i \Delta t \ \right) \tag{5}$$

where, $Q(t)$ is the ordinate of the hydrograph at time t; $u(\Delta t, t)$ is the ordinate at time t of the UH of duration Δt; I_i is the intensity of the rainfall excess during block i of the storm and n is the total number of blocks of precipitation excess. The Clark's UH model provided an opportunity to relate the catchment characteristics to the time of travel, construed as a hydraulic flow parameter synonymous to time of concentration. The translation hydrograph was then determined from a time-area relationship based on eqn. (6).

$$\frac{A(t)}{A_T} = \begin{cases} 1.414\left(\frac{t}{t_c}\right)^{1.5} & for \quad t \le \frac{t_c}{2} \\ 1 - 1.414\left(1 - \frac{t}{t_c}\right)^{1.5} & for \quad t > \frac{t_c}{2} \end{cases} \tag{6}$$

where, the area of the sub-catchment contributing to runoff at time t was represented by $A(t)$ while A_T was the total area. Since changes in land cover conditions were likely to modify the flow paths and hence travel time, a relationship between it and the CN was made following the procedure of Straub [11]. The procedure assumed that t_c was approximately 1.67 times the lag time and estimated the parameter largely from the geometric properties and the mean curve number (CN_m) of the catchments. This was achieved by using a similar approach provided by Sabol [12] based on the relationship provided in eqn. (7).

$$\frac{t_c}{R} = 1.46 - 0.0867 \frac{L_h^{\,2}}{A} \tag{7}$$

where, R is the storage coefficient, t_c is the time of concentration, L_h is the hydraulic length of the catchment and A is the area of the sub-catchments.

3.3 Runoff routing

To evaluate the effects of the land cover change scenarios within the entire basin, estimates of the baseflow discharge for the final outlet of the basin were assumed at bank full discharge. The decay of this flow with time was consequently modeled using the lumped empirically fitted exponential recession model (Pilgrim and Cordery [13]) in eqn. (8).

$$Q_t = Q_0 k^t \tag{8}$$

where, Q_0 is the initial baseflow discharge at time zero (m^3s^{-1}) and k is an exponential decay constant.

The effects of the incoming direct runoff hydrographs within the stream channel were modeled using the physically based Muskinghum-Cunge hydrologic flow routing model. Since a lumped modeling approach was more feasible for the study, the relevant datasets for this model were derived at selected and representative reaches within the sub-catchments. Empirically, the Muskinghum-Cunge model simulated flow based on the principle of mass conservation as shown in eqn. (9).

$$\frac{I_1 + I_2}{2}\Delta t - \frac{O_1 + O_2}{2}\Delta t = S_1 - S_2 \tag{9}$$

where I_1 and I_2 are the inflow discharges at times (1) and (2) in m^3/s and O_1 and O_2 are the outflow discharges at times (1) and (2) in m^3/s, Δt is the time difference between the flows in seconds, S_1 and S_2 are the storage values in the reaches at times (1) and (2) in m^3/s. The relationship between storage, inflow and outflow at the river reach under consideration was further represented as shown in eqn. (10).

$$S = K\left\{XI + (1 - X)O\right\} \tag{10}$$

where, S is the storage, K is a constant in seconds and X is a dimensionless weighting factor. The storage constant parameter and the weighting factor were further related to the hydraulic properties of the reaches based on the appropriate empirical relationships (Cunge [14]; Chow *et al.* [8]; Viessman *et al.* [15]. The Manning's mean flow velocity was obtained based on eqn. (11).

$$v_m = \frac{1}{n} R_h^{2/3} s_o^{1/2} \tag{11}$$

where, v_m is the Manning's mean velocity, n is the dimensionless manning roughness coefficient, R_h is the hydraulic radius in meters and s_o is the channel slope in m/m.

4 Results and discussion

4.1 Spatial analysis and model parameters

The general temporal trends of the changes derived from images showed that conversion from forest to agricultural was prevalent in the basin. The three land

cover scenarios represented extreme alternatives with almost full deforestation on one side and maximum reforestation on the other. The results from each scenario when compared with the ones from the actual land cover in 2008 were as shown in Figure 3. From the comparison, the scenario that best suited each sub-catchment in as far as reducing flood runoff was concerned could be easily identified.

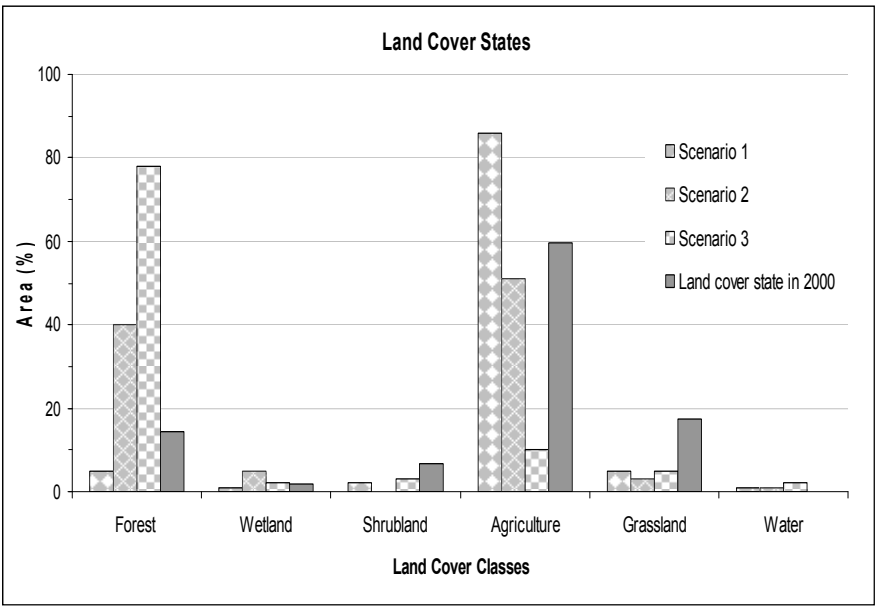

Figure 3: Land cover classes.

In the first scenario, the sub-catchments comprised of 86% agriculture and 5% grassland and forest, respectively. The second scenario exemplified a more or less agricultural and forested catchment, comprising of 40% agriculture and 51% forest. The third scenario was an extreme case with 78% forest and only 10% agriculture.

The major geo-physical and model parameters derived from the spatial datasets were as shown in Table 1.

Based on the general model assumption that higher CN yields higher runoff estimates, it could be seen from the table that an agricultural scenario (sc. 1) provided more runoff compared to the rest. The most vulnerable regions in the basin were sub-catchments No. 9, 12 and 13. Sub-catchment No. 11 indicated the longest hydraulic length due to its relative size and shape. Since changes in the state of land cover were likely to modify flow paths and storage capacities of the region, this study chose to relate these parameters to the derived composite curve numbers and the sub-catchment characteristics. With this, sub-catchments No. 5 and No. 14 exhibited the highest time of concentration and storage capacities in the basin.

Table 1: Geo-physical and model parameters of the sub-catchments.

Id	Area	Average slope	Hydraulic length	Composite Curve Numbers			Time of concentration		
	(km^2)	(%)	(km)	(%)			(h)		
				Sc.1	Sc.2	Sc.3	Sc.1	Sc.2	Sc.3
1	73.7	15	8	80.6	66.6	62.1	1.6	2.4	2.7
2	77.2	18.7	8.9	81.2	70.6	63.4	3	4.1	5
3	130.7	13.2	6.9	77.6	70.3	64.5	4.2	5.2	6
4	147.7	16.6	6.7	78	70.6	64.5	3	3.7	4.4
5	45.3	12	4	80.5	71.5	65.2	4.7	6.1	7.2
6	285.6	8	10.4	78.3	68.7	61.9	1.3	1.7	2
7	365.3	17.2	14.7	79.4	70	63.7	1.8	2.4	2.8
8	446.4	18.4	17.7	72.5	65.5	61.9	2.3	2.8	3.1
9	83.4	12.7	6.3	84.6	75.5	68.8	3.9	5.2	6.3
10	28.4	13.7	4.6	81.7	74.3	65.7	1.5	1.8	2.3
11	747.6	13.5	23.9	78.2	71.6	64.6	1.9	2.3	2.8
12	220.6	6.2	11.5	83.4	74.5	68.8	2.9	3.8	4.4
13	61.2	2.2	7.4	83.3	73.3	63.6	1.1	1.5	2
14	830.5	6.5	18.5	80.7	72.4	66.4	5.4	6.9	8.1

4.2 Runoff volume

The flood hydrograph shown in Figure 4 illustrated how the scenarios in sub catchment No. 2 compared in terms of flood peak discharges and volume.

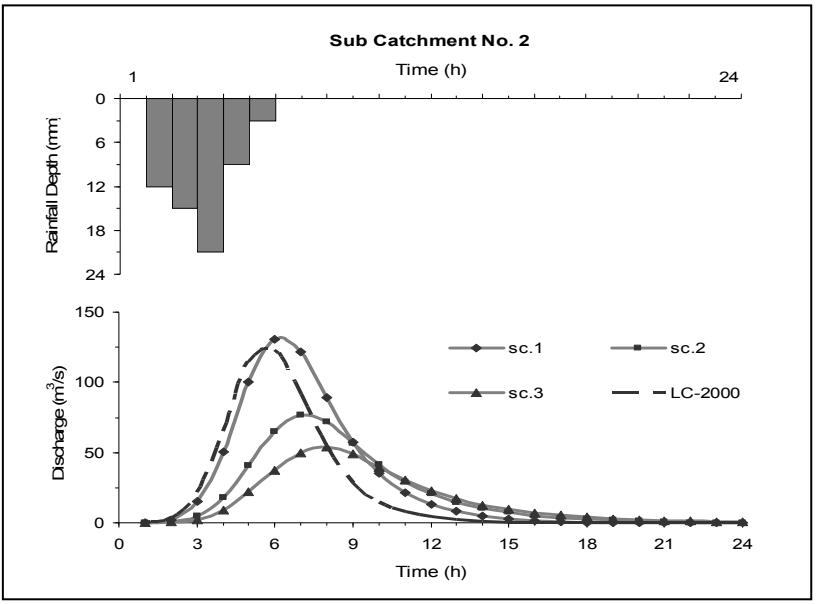

Figure 4: Hydrographs for the 60 mm synthetic storm for selected sub-catchments.

Sub-catchment No. 2 was located in the middle-upland of the basin. This area generally witnessed one of the highest conversion rates of forestland into commercial agriculture. The results indicated that if scenario 1 was applied, this area would experience an increase in peak discharges as compared to the remaining two, given the results of the land cover state in 2008. In terms of flood runoff volume however, scenario 3 would be the most appropriate for the sub-catchments. To distinguish the characteristics of floods in this study, emphasis was placed on the flood volumes in evaluating the simulated runoff which were as shown in Table 2.

Table 2: Simulated runoff volumes for the sub-catchments ($x10^6$ m^3).

	Simulated storm(40mm)				Simulated storm (60mm)				Simulated storm (80mm)			
Id	sc1	sc2	sc3	LC-2000	sc1	sc2	sc3	LC-2000	sc1	sc2	sc3	LC-2000
1	1	0.88	0.79	0.96	1.4	1.22	1.06	1.34	1.49	1.3	1.12	1.43
2	5.55	4.43	3.96	4.22	10.62	8.66	7.8	8.28	11.75	9.62	8.68	9.21
3	2	1.55	1.32	1.88	3.26	2.56	2.16	3.08	3.53	2.79	2.35	3.34
4	2.29	1.8	1.5	2.03	4.23	3.4	2.86	3.79	4.65	3.76	3.17	4.18
5	1.97	1.55	1.28	1.65	3.67	2.95	2.48	3.12	4.04	3.27	2.76	3.44
6	0.83	0.63	0.52	0.8	1.47	1.13	0.94	1.4	1.6	1.24	1.04	1.54
7	4.4	3.2	2.6	3.54	8.16	6.14	5.05	6.73	8.98	6.8	5.61	7.45
8	1.36	0.96	0.78	1.09	2.46	1.8	1.47	2.01	2.7	1.99	1.63	2.21
9	5.88	4.3	3.54	4.46	10.82	8.18	6.82	8.45	11.9	9.05	7.57	9.35
10	2.18	1.84	1.63	2.37	3.09	2.55	2.18	3.37	3.29	2.71	2.31	3.58
11	5.06	3.95	3.45	4.92	8.36	6.6	5.73	8.15	9.07	7.18	6.25	8.84
12	11.51	9.22	7.41	9.54	21.31	17.5	14.29	18.02	23.46	19.35	15.9	20
13	1.31	0.85	0.76	1.12	2.34	1.58	1.4	2.04	2.57	1.75	1.55	2.24
14	14.79	11.15	9.19	14.48	26.38	20.36	16.88	25.89	28.92	22.5	18.7	28.4

Based on the simulated results, various sub-catchments responded differently to the land cover scenarios. To identify the best options suited for reducing flood runoff in the region, a relative reduction of not less than 10% to filter out cases where more than one option could be applicable for a region was adopted. Based on this criterion, it was noted that runoff reduction was more feasible in most regions under scenario 2. However, in sub-catchments Nos. 1, 5, 7, 9 and 12, scenario 3 was noted to fulfill the criteria, where the runoff volume was less than the defined criteria. Generally, in cases where two scenarios could fulfill the above criteria within a sub-catchment, the scenario with the smallest possibility was selected. Figure 5 illustrated the distribution of the land cover states under scenario 2 considered to be the most appropriate in reducing the flood runoff in sub-catchment No. 6 and the actual land cover state in 2008.

In this sub-catchment, the assumed moderate agricultural-forested scenario would hence be applicable in reducing flood flows. This may involve utilizing the area currently under shrublands (10%) and part of the area under grasslands (16%).

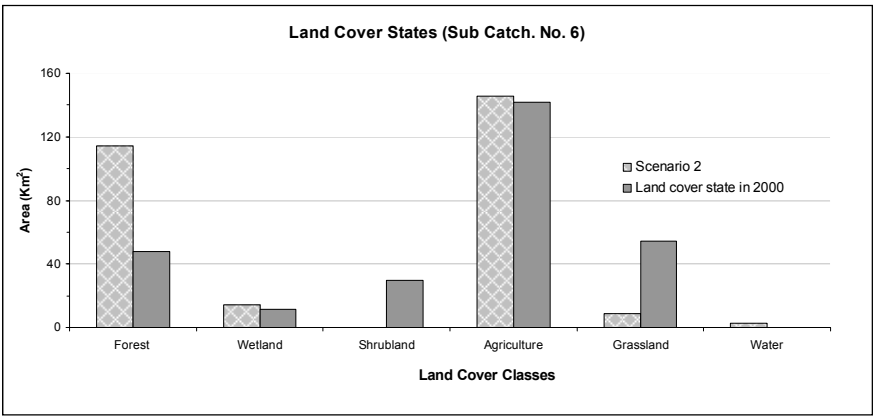

Figure 5: Land cover in sub-catchment No. 6.

4.3 Flood routing

The overall direct runoff produced by the three scenarios in the entire basin was as shown in Table 3. However, to further understand how the basin would respond if either scenario 2 or 3 were applied to the respective sub-catchments, a control scenario named RM-scenario (RM-sc.) was included in the simulations.

Table 3: Routed runoff volumes within the entire basin.

Rainfall depth (mm)	Flood Runoff Volumes ($x10^6 m^3$)				
	LC 2000	Scenario 1	Scenario 2	Scenario 3	RM-sc
40	51.75	58.85	45.41	37.81	43.46
60	93.45	105.22	82.76	69.30	79.37
80	102.86	115.30	91.09	76.79	87.78

Increases of approximately 14%, 13% and 12% were noted from the 40 mm, 60 mm and 80 mm synthetic storms respectively. A forested land cover was noted to significantly reduce direct runoff volume in the basin. The simulated values from the 40 mm, 60 mm and 80 mm synthetic storms generally conformed to decreases by 27%, 26% and 25% respectively.

5 Conclusions and recommendation

Changes in land cover influenced the hydrologic processes in the basin. The general trends of derived land cover changes showed that conversion from forest to agriculture was prevalent. The three land cover scenarios developed

represented extreme alternatives with almost full deforestation on one side and maximum reforestation on the other. In the first scenario, the sub-catchments comprised of 86% agriculture and 5% grassland and forest, respectively. The second scenario exemplified a more or less agricultural and forested catchment, comprising of 40% agriculture and 51% forest. The third scenario was an extreme case with 78% forest and only 10% agriculture. In the entire basin, it was observed that a largely agricultural basin would result into increased flow volume leading to greater floods. On the contrary, a more forested land cover scenario reduced peak discharges and flood volume to levels that could be accommodated by the river channels. Increases of approximately 14%, 13% and 12% was noted from the 40 mm, 60mm and 80 mm synthetic storms respectively. Since the three land cover states did not take into account the demographic and other socio-economic variables likely to dictate the land cover dynamics, it was recommended that such factors be considered in future definitions of the feasible land cover scenarios likely to be tested for their hydrological effects.

Acknowledgements

The authors would like to acknowledge the support of the Austrian Exchange Service (ÖAD) for funding the study. We are grateful to relevant authorities at Lake Victoria Environment and Monitoring Program (LVEMP) and the International Centre for Research in Agroforestry (ICRAF) in Kenya for providing valuable data.

References

[1] Kundu, P.M., Chemelil, M.C, Onyando, J.O, & Gichaba, M., The use of GIS and remote sensing to evaluate the impact of land cover and land use change on discharges in the River Njoro Watershed, Kenya. *Journal of World Association on Soil Water Conservation* J2: 109-120, 2008

[2] Mutua, B.M., & Klik, A., Predicting daily streamflow in ungauged rural catchments: the case of Masinga catchment, Kenya. *Hydrological Sciences* 52(2), 292-304, 2007

[3] Onyando, J.O., Olang, L.O & Chemelil, M.C., Regional Analysis of Conceptual Rainfall-Runoff models for runoff simulation in ungauged catchments of Kenya. *Journal of Civil Engineering Research and Practice* (JCERP), 2(1): 23-37, 2005.

[4] Luke, O.O., Kundu. P, Bauer, T, & Fürst, J., Analysis of spatio-temporal land cover changes for hydrological impact assessment within the Nyando River Basin of Kenya. *Environ Monit Assess*. DOI 10.1007/s10661-010-1743-6, 2010.

[5] Fürst, J., GIS in Hydrologie und Wasserwirtschaft. Herbert Wichmann Verlag, Heidelberg, Germany, 2004.

[6] Batjes, N.H., & Gicheru, P., Soils data derived from SOTER for studies of carbon stocks and change in Kenya (GEF-SOC Project; Version 1.0).

Technical report No. 01, ISRIC – World Soil Information, Wagenigen, The Netherlands, 2004.
[7] NRCS., National Engineering Handbook. Hydrology (section 4). Soil Conservation Service, US Department of Agriculture: Washington, DC, USA, 1972
[8] Maidment, D.R., *Handbook of hydrology*, McGraw Hill, New York, San Francisco, USA, 1993.
[9] Chow, V.T., Maidment, D.R., & Mays, L.W., *Applied Hydrology,* McGraw-Hill, New York, USA, 1988.
[10] USACE, Flood Runoff analysis. *Engineering Manual,* No. 110-2-1417. Washington. USA, 1994.
[11] Straub, T.D., Melching, C.S., & Kocker, K.E., Equations for estimating Clark Unit-hydrograph parameters for small rural watersheds in Illinois. US. Geological Survey Water-Resources Investigations Report 00-4184, 2000.
[12] Sabol, G.V., Clark unit hydrograph and parameter estimation. *Journal of Hydraulic Engineering*, 114(1): 103–111, 1988.
[13] Pilgrim, D.H, & Cordery, I., Flood runoff. In: DR Maidment (Editor). *Handbook of Hydrology*, McGraw-Hill, New York, USA, 1992.
[14] Cunge, J.A., On the Subject of a Flood Propagation Computation Method (Muskingum Method). *Journal of Hydraulic Research* 7(2): 205-230, 1969.
[15] Viessmann, W., Lewis, G.L., & Knapp, J.W., *Introduction to Hydrology*, Harper Collins. New York, USA, 1989